Physicochemical Properties and Morphology of Fluorocarbon Films Synthesized on Crosslinked Polyethylene by Capacitively Coupled Octafluorocyclobutane Plasma

ARTICLE *in* THE JOURNAL OF PHYSICAL CHEMISTRY C · FEBRUARY 2007

Impact Factor: 4.77 · DOI: 10.1021/jp067521e

2 AUTHORS, INCLUDING:

Satomi Tajima
Toyota Central R & D Labs., Inc.
26 PUBLICATIONS **147** CITATIONS

SEE PROFILE

Physicochemical Properties and Morphology of Fluorocarbon Films Synthesized on Crosslinked Polyethylene by Capacitively Coupled Octafluorocyclobutane Plasma

S. Tajima and K. Komvopoulos*

Department of Mechanical Engineering, University of California, Berkeley, California 94720

Received: November 13, 2006; In Final Form: January 8, 2007

Capacitively coupled octafluorocyclobutane (C_4F_8) plasma was used to synthesize fluorocarbon films on low-density polyethylene, which was surface-crosslinked by treatment with inductively coupled Ar plasma. The dependence of the thickness, surface morphology, and chemical characteristics of the fluorocarbon films on the plasma power was studied under different plasma conditions. Significantly lower deposition rates were obtained under the sole effect of uncharged particles (shielded plasma conditions). Microscale and nanoscale film growth characteristics were examined at different levels of energy/monomer mass. A significant increase in hydrophobicity was observed under shielded plasma conditions as a result of the higher fluorine concentrations of the deposited films. The film chemical structures were interpreted in terms of the degree of crosslinking. Increasing the exposure of polyethylene to the shielded plasma conditions resulted in the formation of fluorocarbon films with hybrid chemical structures consisting of a crosslinked interfacial layer covalently bonded to the polymer substrate and a hydrophobic compliant surface layer rich in CF_2 groups. The results of this study illustrate the potential of shielded plasma treatment to tailor the chemical structure of thin fluorocarbon films.

Introduction

Fluorocarbon (FC) film deposition by different plasma techniques has been used in numerous electrical, mechanical, and biomedical applications mainly due to the desirable physicochemical properties (e.g., dielectric constant, surface energy, friction, and wettability) and hemocompatibility of FC films. Recent studies dealing with FC plasmas have shown that film growth is controlled by C_xF_y ions and neutrals.[1−3] For efficient FC film deposition, large monomer precursors (e.g., C_3F_8 and C_4F_8) are desirable because they produce more C_xF_y ions and neutrals than small monomer precursors (e.g., CF_4, C_2F_4, and C_2F_6).[1,3,4]

The FC film properties depend on their chemical composition, which differs from that of the film precursors. FC films with different CF_3, CF_2, CF, and CCF concentrations can be synthesized, depending on the ion bombardment intensity and vacuum ultraviolet (VUV) and ultraviolet (UV) radiation. In addition, the presence of secondary precursors, such as H_2, O_2, and Ar, may also affect the chemical composition of FC films.[5−8] For example, CF_2-rich FC films with uncrosslinked microstructures (Figure 1(a)) can be deposited under low intensities of ion bombardment and VUV/UV radiation,[9] while films rich in CF and CCF groups exhibiting two-dimensional branching and/or crosslinked microstructures (Figure 1(b)) can be obtained under plasma conditions of intense ion bombardment and VUV/UV radiation.[5] CF_2-rich films produced by downstream plasma treatment demonstrated increased thromboresistance[10,11] and lower surface energy[12] than CF- and CCF-rich films. More recently, CF_2-rich films were deposited on a Si wafer that was shielded from the plasma.[7] The advantage of shielded plasma over pulsed or downstream plasma is that the treatment conditions can be varied without changing the power supply or chamber configuration.

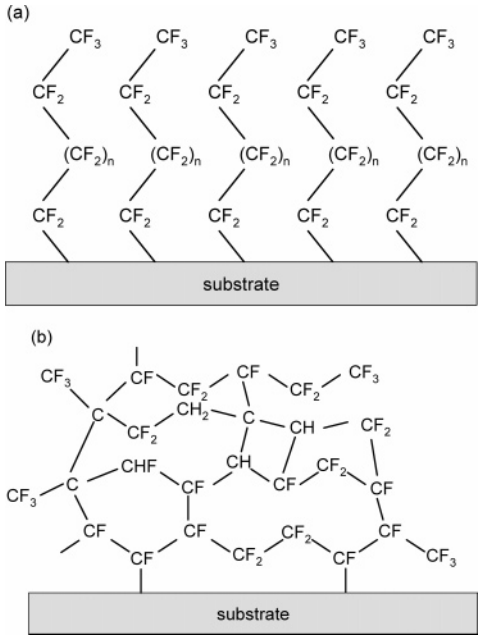

Figure 1. Chemical structures of typical fluorocarbon films grown under conditions of (a) low-intensity plasma (ref 9) and (b) high-intensity plasma (ref 5).

The ion bombardment intensity exhibits a strong effect on the deposition rate (film thickness), which can be correlated with the energy/monomer mass *W*/*FM*, where *W* is the plasma power, *F* is the flow rate, and *M* is the molecular weight of the film precursor.[13,14] The film thickness increases with *W*/*FM* up to a threshold value above which it decreases due to film etching resulting from the intensified ion bombardment.[13,14] However,

* Corresponding author. E-mail: kyriakos@me.berkeley.edu. Tel.: (510)-642-2563. Fax: (510)-643-5599.

10.1021/jp067521e CCC: $37.00
Published on Web 03/01/2007

the film growth dependence on *W/FM* has not been examined in the absence of ion and VUV/UV radiation effects.

The surface roughness of the deposited films can be affected by the film precursors. For example, films synthesized on Cu-coated Si wafers from C_4F_8 plasma demonstrated lower roughness than those obtained from other precursors, such as C_3F_6 and C_2F_3H.[15,16] Contrary to the surface chemistry and the thickness of FC films, the modification of the surface topography under different plasma conditions has not been explored thoroughly.

The majority of previous studies investigated the surface microtopographies of films grown on smooth Si or glass substrates; however, knowledge of nanoscale film growth mechanisms is sparse. Because the film surface morphology and growth mechanisms depend strongly on the substrate material, the results for very smooth substrates may not be applicable for relatively rough polymer surfaces. Moreover, in-depth analysis of the multiscale surface topography of FC films grown on polymer substrates has not been presented to date. In particular, the role of energetic ions in the modification of the surface topography of FC films has not attracted research attention. Intense ion bombardment due to high power treatment not only leads to etching of the FC film but also induces significant surface roughening. Since the film roughness is of great importance in many leading-edge technologies, fundamental studies of the effects of plasma conditions on the micro-/nanotopography of FC films is of great significance.

In this study, smooth FC films were synthesized on surface-crosslinked, low-density polyethylene (LDPE) by capacitively coupled octafluorocyclobutane (C_4F_8) plasma treatment. Differences in the nanoscale and microscale film growth mechanisms on LDPE samples with or without a plasma shield were investigated in a wide range of plasma power. Results for the film thickness, wettability, and surface chemistry are interpreted in terms of corresponding plasma conditions to elucidate the effects of plasma species, such as ions, VUV/UV radiation, and uncharged particles, on the growth, morphology, and physicochemical properties of the FC films.

Experimental Procedures

Polyethylene Specimens. Specimens of 1 cm diameter and thickness in the range of 800−900 μm were fabricated by press casting pellets of LDPE (Sigma-Aldrich, St. Louis, MO) onto atomic force microscope (AFM) metal disks. X-ray diffraction and differential scanning calorimetry demonstrated that the crystallinity of the LDPE specimens was equal to ~50%. To induce surface crosslinking, the specimens were exposed to plasma generated from a radio frequency (rf) inductively coupled plasma source (Litmas Inc., Charlotte, NC). The plasma was produced from a high-purity (99.999%) Ar gas (Praxair, Danbury, CT) introduced into the vacuum chamber at a flow rate of 100 sccm under a pressure of 500 mTorr. All the specimens were treated for 15 min under plasma conditions of 1200 W rf power and sample-to-plasma source distance equal to 15 cm, producing an ion energy fluence of 1.8×10^5 J/m^2. More details for the experimental setup and the modification of the physicochemical properties of LDPE under different Ar plasma conditions can be found elsewhere.[17−19]

Fluorocarbon Film Deposition. FC films were grown on surface-crosslinked LDPE specimens in a rf capacitively coupled plasma reactor (RTE73 AMNS-500-E, Plasmatherm Inc., Kresson, NJ) with 29.4 cm plate diameter and plate-to-plate distance equal to 5 cm. The specimens were placed on the grounded (bottom) electrode, which was water-cooled to maintain a substrate temperature of 16−17 °C. The reaction gas (C_4F_8) was introduced into the chamber at a flow rate of 50 sccm 2 min before initiating film deposition to establish a stable base pressure of 85 mTorr. Film deposition was then performed under conditions of rf power in the range of 50−450 W and working pressure between 85 and 122 mTorr (depending on the power). In all the experiments, the deposition time was fixed at 2 min, except one experiment in which it was 30 min. The specimens were kept under a pressure of 85 mTorr for 1 min after the film deposition to allow active plasma species to gradually reach equilibrium before turning off the power. The plasma conditions of all the FC film depositions examined in this study are given in Table 1.

TABLE 1: Density of Uncharged Particles in the Plasma, Energy/Monomer Mass, and Film Thickness (Shielded Plasma Conditions) Measured by Angle-Resolved XPS versus Plasma Conditions

plasma conditions[a]		density of uncharged particles	energy/monomer mass	film thickness
power W (W)	pressure P (mTorr)	n_g ($\times 10^{17}$)	W/FM (MJ/kg)	t (nm)[b]
50	85	1.0	7.4	Ø
100	84	1.0	14.7	Ø
150	86	1.0	22.1	0.26
200	86	1.0	29.4	1.1
250	95	1.1	36.8	1.3
275	96	1.1	40.4	1.6
300	95	1.1	44.1	2.1
450	120	1.5	66.2	2.5

[a] Deposition time = 2 min. [b]Shielded plasma conditions (Ø ≡ incomplete film coverage).

In a series of plasma treatments, the specimens were shielded from the plasma by a 2.54 × 2.54 cm Al plate, which was placed 2 mm above the specimen surface to prevent ion bombardment and VUV/UV radiation during film growth. The distance from the specimen center to the shield edge was 7.4 mm. Hereafter, the plasma environment obtained with and without the Al shield will be referred to as "shielded" and "unshielded" plasma, respectively. The survival rate of CF_x^+ ($x = 1$, 2, or 3) ions of incident energy in the range of 30−150 eV after surface impingement is less than 6%.[20,21] Hence, most ions were either absorbed or scattered as uncharged particles after impinging onto the surface of the Al shield. Therefore, only uncharged particles interacted with the crosslinked polymer surface during film growth under shielded plasma conditions.

Microanalysis Techniques. The FC film thickness, surface roughness, and changes in the wettability and chemical characteristics of Ar-treated (crosslinked) LDPE due to FC film deposition were examined with an AFM, ellipsometer, spectroscopic reflectometer (SR), X-ray photoelectron spectroscope (XPS), and goniometer. All the film characterization studies were performed within 0.5−3 h from the film deposition to avoid any aging effects on the measurements.

Film Thickness. The thickness of the FC films grown under unshielded plasma conditions was measured with an ellipsometer (AutoEL II, Model A9822, Rudolph Technologies, Inc., Flanders, NJ) with a wavelength of 633 nm and a SR (210 XP Scanning UV Nanospec/DUV Microspectrophotometer, Nanometrics Inc., Milpitas, CA). The films were deposited on 10 cm diameter p-type Si(100) wafers approximately 5 min after treating the wafers with 49% HF for 10 min to remove the native oxide layer. Average and standard deviation values of each film thickness were obtained from ten measurements. Differences in the film thickness estimated with the previous techniques were on the order of the experimental scatter (standard deviation).

The FC film thickness t and refractive index were calculated from the measured ellipsometry parameters using customized software (double-layer absorbing film (DAFIBM)). The refractive index of the FC films synthesized under different plasma conditions was found to be in the range of 1.38−1.43, consistent with previous results.[22] Film thickness measurements were obtained with an accuracy of ±3 Å, assuming a film refractive index of 1.4. The same refractive index value was used to estimate the film thickness from the SR measurements.

In view of the very thin FC films grown under shielded plasma conditions, the film thickness was determined from angle-resolved XPS or ellipsometry measurements. XPS spectra were acquired with a Perkin-Elmer PHI 5400 ESCA system (without charge neutralization or monochromator) using Al−Kα (1486.6 eV) X-ray source and a 54.7° angle relative to the analyzer axis. The sampling depth h is given by

$$h = 3\lambda \sin\theta \tag{1}$$

where λ is the inelastic mean free path (λ = 2.5 nm for FC films)[12] and θ is the take-off angle measured from the surface normal. XPS spectra were acquired from different depths (0−7.5 nm) by varying θ between 0° and 90°. Survey spectra were collected in the binding energy range of 0−270 eV with 187 eV pass energy and 0.5 eV resolution. The film thickness was determined from the depth at which the peaks corresponding to the Si substrate (Si2s and $Si2p_3$) disappeared from the XPS spectrum.

Film Surface Morphology. The morphology of the FC films at various length scales was studied with an AFM (NanoScope IV, Veeco Metrology, Santa Barbara, CA) operated in the contact mode. AFM images were obtained with a pyramidal Si tip of nominal radius of curvature less than 10 nm and microcantilever stiffness of 0.12 N/m. A low contact force of 10−50 nN was applied during scanning to minimize the surface damage. AFM scans of 1 × 1 and 10 × 10 μm^2 surface areas were obtained with a resolution of 256 × 256 pixels (i.e., pixel-to-pixel distance (sampling length) equal to 3.9 and 39.2 nm, respectively). The sampling length indicates the scale at which the roughness parameters were determined from the AFM images. Thus, it may be presumed that the 1 and 100 μm^2 area scans are indicative of the nanoscale and microscale surface topographies of the FC films. Statistical surface topography parameters, such as centerline average roughness R_a, root-mean-square roughness R_q, skewness, and kurtosis, calculated from 1 and 100 μm^2 AFM surface scans were used to quantify the changes in the film surface topographies. For statistical analysis, surface roughness parameters were calculated as averages of six measurements obtained from two or three specimens of the same FC film.

Film Surface Chemical Analysis. To examine the variation of the FC film wettability with the plasma power, static contact angle measurements were performed at room temperature using a drop shape analysis system (DSA10, Krüss GmbH, Hamburg, Germany). Average contact angles were calculated from four contact angle measurements obtained from four specimens of the same FC film (i.e., 16 contact angle measurements for each film).

Film chemical compositions were determined from XPS spectra of 1 mm diameter sampling surface area and 5.3 nm depth using an electron take-off angle θ = 45°. Survey spectra were collected with pass energy of 187 eV and resolution of 1.0 eV to identify the elements present on the surfaces. For chemical bond identification, detail scans of core level C1s, O1s, and F1s were collected with pass energy of 35.75 eV and resolution of 0.05 eV. To compensate for surface charging effects, all binding energies in the C1s core level spectra were referenced to the $\underline{C}F_2$ peak centered at 291.5 eV or the $\underline{C}$-H/$\underline{C}$-C peak centered at 285.0 eV. After Shirley background noise subtraction, polar functionalities were determined by curve fitting the C1s spectra with 70% Gaussian−30% Lorentzian (GL) distributions of full width at half-maximum equal to 2.0 eV (AugerScan 3, RBD Enterprises, Inc., Bend, OR). A goodness-of-fit parameter (corresponding to the error-mean-square parameter) of less than 3 was used in the curve fitting algorithm. Table 2 shows the peak positions of the C-F bonds used to curve fit the C1s spectra.[23−25]

TABLE 2: Binding Energy of Functional Groups Identified by Gaussian−Lorentzian Curve Fitting of the C1s Core Level XPS Spectra

group designation	functional groups[a]	binding energy (eV)
$-\underline{C}F_3$	$-\underline{C}F_3$, $\underline{C}F_3-CF$	293.5
$-\underline{C}F_2-$	$-\underline{C}F_2$, $-\underline{C}F_2-CF-$, $-CF_2-\underline{C}F_2-$	291.5
$-\underline{C}F-CF_n$	$-\underline{C}F-CF_2$, $-\underline{C}F-CF-CF-$, $CF_3-\underline{C}-CF_3$	289.9
$-\underline{C}F-$	$-\underline{C}F-$	288.7
$-\underline{C}-CF_n-$	$-\underline{C}-CF_2$, $-\underline{C}-CF_3$, $-CF-\underline{C}-CF-$, $-CF-\underline{C}-CF_2-$	286.9
$-\underline{C}-C-$	$-\underline{C}-C-$, $-\underline{C}-H-$	285.0

[a] Refs 23 and 24.

The FC films synthesized by capacitively coupled C_4F_8 plasma are hybrids of the two chemical structures shown in Figure 1. The concentration of each structure in the FC film was determined from the degree of crosslinking, evaluated in terms of the F/C ratio, percent of crosslinking, and connectivity number. The F/C ratio was calculated from the curve-fitted C1s spectra using the relationship[26]

$$F/C = [3 \times \%\underline{C}F_3 + 2 \times \%\underline{C}F_2 + 1 \times \%\underline{C}F\text{-}CF_n + 1 \times \%\underline{C}F]/100 \tag{2}$$

where n = 1, 2, or 3. The weighting factor (1, 2, or 3) of each term in eq 2 denotes the number of F atoms attached to each underlined C atom. The higher the F/C ratio, the more F atoms attached to C atoms and, hence, the lower the degree of crosslinking.

The degree of crosslinking is proportional to the sum of the areas under the $\underline{C}F$-CF_n, $\underline{C}F$, $\underline{C}$-CF_n, and $\underline{C}$-C/$\underline{C}$-H peaks divided by the total area under the C1s peak. This is because only these chemical bonds contribute to chain crosslinking. Thus, the percent of crosslinking X can be expressed as[27]

$$X = \frac{\%\underline{C}F\text{-}CF_n + \%\underline{C}F + \%\underline{C}\text{-}CF_n + \%\underline{C}\text{-}C}{100} \tag{3}$$

Because the average connectivity number m represents the average number of network-forming bonds per atom, it can be used to evaluate the rigidity of an amorphous material.[28,29] Thus, the FC film rigidity was examined by considering the number of bonds available to other carbon atoms,[26] using the relationship

$$m = [1 \times \%\underline{C}F_3 + 2 \times \%\underline{C}F_2 + 3 \times \%\underline{C}F\text{-}CF_n + 3 \times \%\underline{C}F + 4 \times \%\underline{C}\text{-}CF_n + 4 \times \%\underline{C}\text{-}C]/100 \tag{4}$$

where the weighting factor (1, 2, 3, or 4) of each term in eq 4 indicates the number of available bonds in each underlined C atom. For rigid atomic bonds characterized by a high degree of

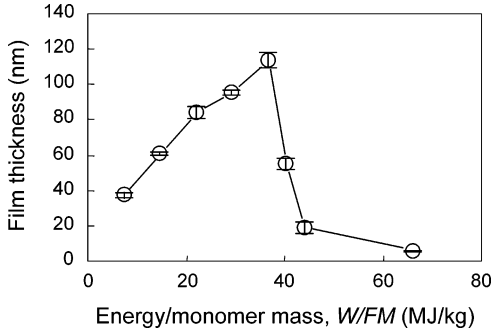

Figure 2. Fluorocarbon film thickness versus energy/monomer mass (unshielded plasma conditions).

crosslinking $m > 2.4$, while for flexible atomic bonds associated with a low degree of crosslinking $m < 2.4$.[26,28] The previously discussed methods (eqs 2−4) were used to determine the F concentration and the degree of crosslinking in each FC film by calculating the areas under the GL distributions fitted to the C1s spectra.

Results and Discussion

Plasma Conditions. Because of the ion density dependence of C_4F_8 dissociation, variations in the plasma power resulted in pressure changes (Table 1). The density of uncharged particles (i.e., neutrals, radicals, metastables, and atoms) in the plasma n_g, determined from the ideal gas law

$$n_g = \frac{PV}{kT} \tag{5}$$

where P is the pressure, V ($= 3.65 \times 10^{-3}$ m^3) is the chamber volume, k ($= 1.381 \times 10^{-23}$ J/K) is the Boltzmann constant, and T (≈ 290 K) is the temperature of the grounded electrode, and the values of the *W/FM* factor calculated for $F = 3.4 \times 10^{-5}$ mol/s ($= 50$ sccm) and $M = 0.2$ kg/mol are given in Table 1. For *W/FM* less than a threshold value (energy deficient region), more energy is needed to form the film than the monomer and the film thickness increases with the plasma power,[14,15] while above the *W/FM* threshold (monomer deficient region), excessive fragmentation of the monomer molecules leads to the formation of highly reactive species (e.g., CF_3^+, CF_3, F) that induce film ablation and the film thickness either remains constant[13] or decreases.[16] High *W/FM* values represent conditions of intense ion bombardment conducive to film etching.[30,31] The threshold *W/FM* depends on the bonding energy of the precursor monomer and the reactor configuration[14] and can be empirically determined from film thickness and roughness measurements.

Film Growth. The thickness of the FC films grown on Si under unshielded plasma conditions versus energy/monomer mass is shown in Figure 2. The film thickness increases with *W/FM* up to ~37 MJ/kg and then decreases sharply in the range of 37−41 MJ/kg, much faster than what was observed in a previous study.[15] This pronounced decrease in film thickness is possibly due to the increased dissociation of F, CF_3^+, CF, and/or CF_3 species which cause film ablation.[15] As the results in Figure 2 show, the transition from energy-deficient region to monomer-deficient region (*W/FM* threshold) for deposition time equal to 2 min is in the range of 36−41 MJ/kg.

The thickness of the FC films synthesized under shielded plasma conditions (determined from angle-resolved XPS) is given in Table 1. The appearance of the Si2s and $Si2p_3$ peaks in the XPS spectra corresponding to the smallest sampling depth for *W/FM* < 15 MJ/kg indicated that these FC films were discontinuous. A steady increase in film thickness was found for *W/FM* > 15 MJ/kg. Thus, a transition from energy-deficient region to monomer-deficient region was not observed in the absence of ion bombardment and VUV/UV radiation.

Differences in the concentration of uncharged particles below the edge and the center of the shield promoted surface diffusion of the uncharged particles. It has been argued that diffusion of uncharged particles is the dominant film deposition process under shielded plasma conditions.[7] According to eq 5, the density of the uncharged particles in the plasma is independent of plasma power. (Although increasing the power from 50 to 450 W resulted in a pressure increase from 85 to 120 mTorr, the effect of this pressure change on the density of the uncharged particles was very small, as shown in Table 1.) However, the thickness of the FC films deposited under shielded plasma conditions increased with the plasma power. This suggests that the former diffusion model,[7] which accounts only for uncharged particles from the plasma, cannot fully describe the film growth mechanism under shielded plasma conditions. Hence, it is necessary to include in the diffusion model the density of the uncharged particles generated from the impingement of energetic ions onto the metal shield. The number of ion−shield collisions depends on the ion density and is proportional to *W/FM*. Experimental evidence suggests that the CF_2 concentration near the plasma-surface interface increases with the ion energy.[20] Thus, uncharged particles produced from ion−shield collisions should play an important role in the deposition of thick films under shielded plasma conditions and high *W/FM*. To investigate this hypothesis, a Si wafer was placed on the ground electrode with one-third of its surface covered by another Si wafer during plasma treatment at a power of 150 W. The film thickness (measured with a SR) versus distance from the shield edge is shown in Figure 3. The higher film thickness near the shield edge is attributed to uncharged particles generated from ion−shield collisions and the smaller film thickness in the exposed area away from the shield edge to the effects of ions and uncharged particles from the plasma. This finding demonstrates that in addition to ions and uncharged particles from the plasma, uncharged particles from ion−shield collisions played an important role in the film deposition process.

The film deposition rate under shielded plasma conditions was much less than that under unshielded plasma conditions. The results shown in Figure 2 indicate that the increase of the deposition rate in the range of *W/FM* < 37 MJ/kg was predominantly due to ions that exhibit a higher adsorption rate than uncharged particles. Above the *W/FM* threshold, excessive ion bombardment promoted film sputtering, resulting in the decrease of the film thickness. Diffusion of uncharged particles from the plasma and ion−shield collisions controlled film deposition under shielded plasma conditions. In this environment, the film thickness increased continuously with *W/FM* (Table 1) due to the absence of ion bombardment.

Film Surface Morphology. Figure 4 shows the surface roughness R_q as a function of *W/FM* for both shielded and unshielded plasma conditions. The roughness range of Ar-treated LDPE is also shown for reference. As mentioned earlier, the roughness data for 100 and 1 μm^2 scan areas can be considered to be representative of the microscale and nanoscale surface topographies. Since the R_a data showed similar trends with those shown in Figure 4 (although on average they were lower by ~27% than the R_q data) they are not presented here for brevity. Both microscale and nanoscale skewness varied between

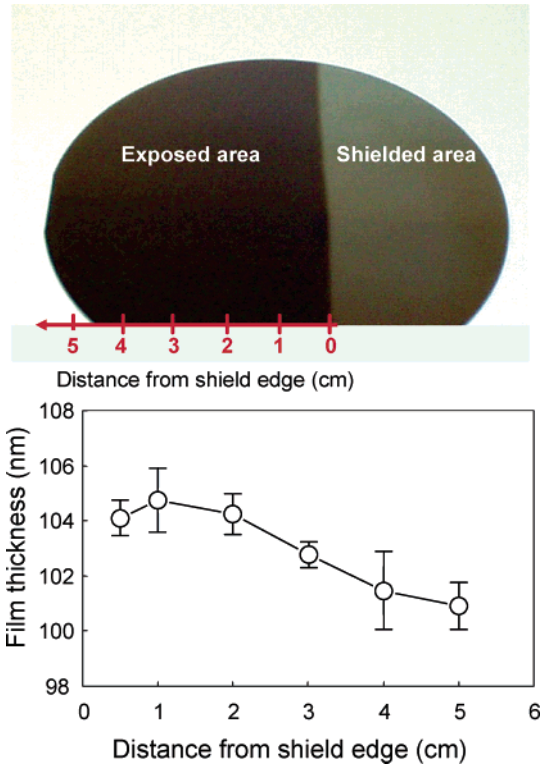

Figure 3. Fluorocarbon film thickness versus distance from shield edge (unshielded plasma conditions). The locations of the exposed area where the film thickness was measured are shown in the photograph above the film thickness plot.

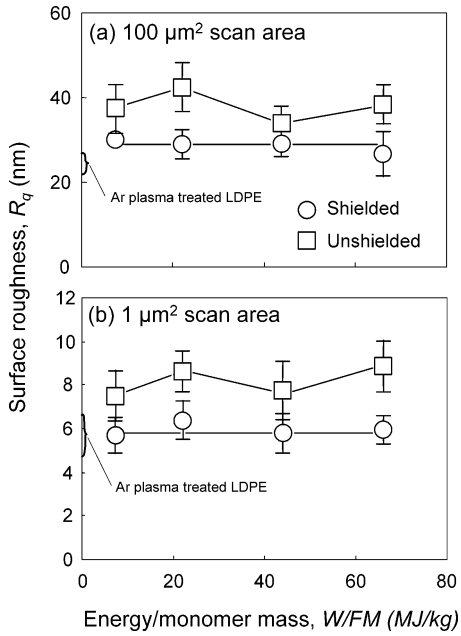

Figure 4. Surface roughness of fluorocarbon films grown under (O) shielded and (□) unshielded plasma conditions: (a) 100 μm^2 and (b) 1 μm^2 AFM surface images.

−0.6 and 0.6, indicating that the asperity heights exhibited Gaussian distributions, while the kurtosis assumed values in the range of 2−5 for both length scales. The film roughness for shielded plasma conditions was close to that of Ar-treated LDPE, especially in the nanoscale roughness measurements. The nanoscale and microscale roughness of the FC films synthesized under unshielded plasma conditions were about 1.2−1.5 times higher than those of the films grown under shielded plasma conditions and that of Ar-treated LDPE over the entire *W/FM*

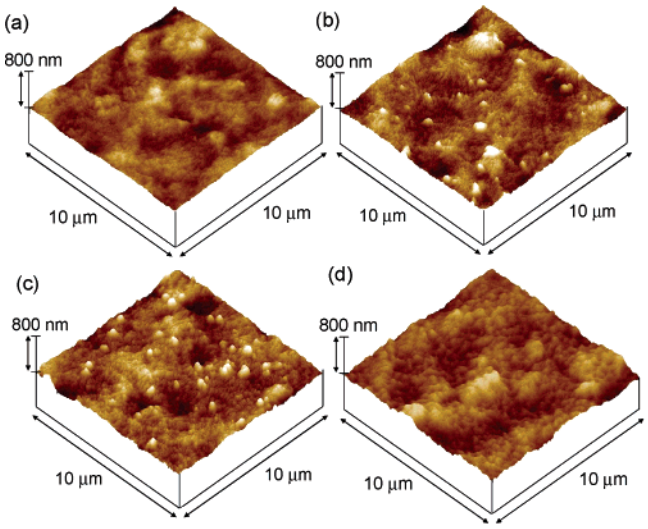

Figure 5. Microscale surface topographies of (a) Ar-treated LDPE and fluorocarbon films grown under (b) shielded plasma conditions (*W/FM* = 66.2 MJ/kg) and (c),(d) unshielded plasma conditions (*W/FM* = 22.1 and 66.2 MJ/kg).

range. For shielded plasma conditions, both R_a and R_q roughness parameters exhibited small fluctuations in the *W/FM* range examined in this study. These roughness variations will be explained later by examining the AFM images of the film topographies.

Qualitative comparisons of surface topography maps provided further insight into microscale and nanoscale roughness changes. Figure 5 shows representative microscale topographies of Ar-treated LDPE and FC films grown under shielded and unshielded plasma conditions. Film microtopographies similar to that of Ar-treated LDPE (Figure 5(a)) were obtained under shielded plasma conditions for *W/FM* ≤ 44.1 MJ/kg. However, high energy/monomer mass (e.g., *W/FM* = 66.2 MJ/kg) lead to the formation of small asperities and nanoparticles that resulted in slight surface roughening (Figure 5(b)). Despite these surface changes, AFM imaging indicated that the underlying morphology of the FC films grown under shielded plasma conditions was similar to that of Ar-treated LDPE. The similar microtopographies of Ar-treated LDPE and FC films deposited under shielded plasma conditions for *W/FM* ≤ 44.1 MJ/kg are consistent with the invariance of microscale roughness under these conditions (Figure 4(a)). The small changes in R_q for *W/FM* = 66.2 MJ/kg are attributed to the formation of small asperities and nanoparticles on the FC film surfaces.

Microscale morphologies of FC films grown under unshielded plasma conditions for relatively low and high energy/molecular mass are shown in Figure 5(c) and (d), respectively. A film morphology similar to that shown in Figure 5(c) was also observed for *W/FM* = 7.4 MJ/kg. On the basis of particle measurements obtained from three different scans, the average particle size and height corresponding to Figure 5(c) was found to be 562 ± 111 and 145 ± 47 nm, respectively. For unshielded plasma conditions, the particle density increased with *W/FM* from 7.4 to 22.1 MJ/kg. Particle formation diminished for *W/FM* > 44.1 MJ/kg, while uniform etch pits emerged for *W/FM* = 66.2 MJ/kg due to the intensified ion bombardment (Figure 5(d)).

Particle formation at high pressures has been attributed to gas-phase polymerization.[15] In the present study, more gas-phase polymerization was encountered for plasma power equal to 150 W than 50 W under a pressure of ~85 mTorr (Table 1). Thus, gas-phase polymerization occurred under conditions conducive

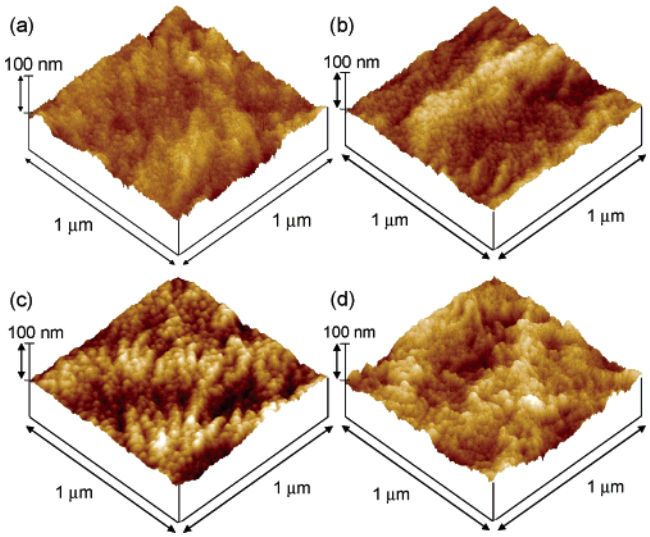

Figure 6. Nanoscale surface topographies of (a) Ar-treated LDPE and fluorocarbon films grown under shielded plasma conditions for (b) *W/FM* = 22.1 MJ/kg, (c) *W/FM* = 44.1 MJ/kg, and (d) *W/FM* = 66.2 MJ/kg.

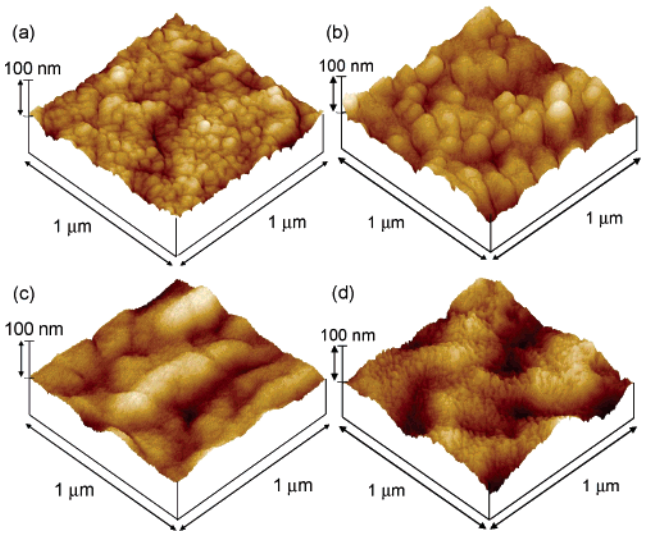

Figure 7. Nanoscale surface topographies of fluorocarbon films grown under unshielded plasma conditions for (a) *W/FM* = 7.4 MJ/kg, (b) *W/FM* = 22.1 MJ/kg, (c) *W/FM* = 44.1 MJ/kg, and (d) *W/FM* = 66.2 MJ/kg.

to the development of high ion density plasma. Excess ion bombardment promoted etching of the polymerized nanoparticles. The particles produced from gas-phase polymerization in this study were much smaller and less dense than those generated from C_3F_6 and C_2F_3H plasmas.[15] In addition to particle formation by microscale gas-phase polymerization, unshielded plasma conditions and *W/FM* < 22.1 MJ/kg yielded numerous asperities of average size and height (determined from measurements obtained from three different scans) equal to 181 ± 27 and 41 ± 7 nm, respectively. Hence, the formation of particles and asperities under unshielded plasma conditions resulted in higher R_q values than those of the Ar-treated LDPE surface (Figure 4(a)).

Figures 4(a) and 5 indicate that nanoscopic particles, asperities, and etch pits were the main surface features of the film microtopographies; however, the effect of these features on the film roughness was marginal. Asperity formation on the film surfaces was encountered under both shielded (Figure 5(b)) and unshielded (Figure 5(c)) plasma conditions. The initial stage of film growth can be described by the Stranski−Krastanov growth model[32] comprising the initial growth of a layer tightly bonded to the substrate and the subsequent formation of asperity islands on this layer surface. In addition to the development of asperity islands, particle formation due to gas-phase polymerization occurred under shielded plasma conditions and high energy/monomer mass (*W/FM* = 66.2 MJ/kg) or unshielded plasma conditions and intermediate to low energy/monomer mass (*W/FM* ≤ 22.1 MJ/kg).

Figures 6 and 7 show representative AFM images of the nanoscale topographies of Ar-treated LDPE and FC films grown under shielded and unshielded plasma conditions. The morphology of Ar-treated LDPE comprises numerous nanoscopic asperities (Figure 6(a)). A comparison of the film surfaces for shielded plasma conditions (Figure 6(b)−(d)) indicates that increasing the energy/monomer mass resulted in asperity coarsening. This is further documented by statistical results of the asperity size and height for shielded plasma conditions given in Table 3. The enlargement of the asperities is attributed to the increase of the density of uncharged particles produced from ion−shield collisions with *W/FM*. The asperity size became less uniform for *W/FM* = 66.2 MJ/kg, probably because of the shadowing effect of the tallest grains, a characteristic feature of the zone 1 growth model.[33] The grains formed under shielded plasma conditions are similar to the zone 1 grains produced from $C_2H_2F_4$ plasma.[34]

TABLE 3: Size and Height of Asperities on the Surfaces of Fluorocarbon Films Grown under Shielded Plasma Conditions

energy/monomer mass *W/FM* (MJ/kg)	asperity size (nm)	asperity height (nm)
Ø[a]	37.0 ± 7.1	9.4 ± 2.5
7.4	36.2 ± 9.5	11.0 ± 3.4
22.1	41.7 ± 9.2	8.6 ± 3.0
44.1	59.4 ± 14.6	11.2 ± 2.4
66.2	95.8 ± 22.6	15.9 ± 5.1

[a] Ø ≡ Ar-treated LDPE.

The nanoscale morphologies of the films grown under unshielded plasma conditions (Figure 7) illustrate the evolution of grain growth with increasing *W/FM*. Grain growth exhibiting a shadowing effect was not observed under unshielded plasma conditions even for the lowest value of energy/monomer mass (7.4 MJ/kg). Instead, polygon grains of average base length equal to 62 ± 20 nm (calculated from 15 grains of three surface scans) were found on the film surface (Figure 7(a)). The formation of such grains on FC films has not been observed previously. These polygon grains were flat and fairly uniform (i.e., similar to those of the zone 3 growth model).[33] Increasing the energy/monomer mass to 22.1 MJ/kg promoted coalescence of a few polygon grains, resulting in larger grains (Figure 7(b)). The different grain structures produced under shielded and unshielded plasma conditions is associated with the increase of the plasma ion energy. Both ion bombardment intensity and heat at the film surface were higher in the unshielded plasma environment and increased much more with *W/FM*. For unshielded plasma conditions at *W/FM* > 44.1 MJ/kg, the surface morphology comprised large and smooth protrusions devoid of grain structures (Figure 7(c)). The increase of the ion bombardment intensity with the plasma power (*W/FM* = 66.2 MJ/kg) resulted in microscale and nanoscale etch pits of average peak-to-valley width equal to 10 nm and depth of 2−3 nm (Figure 7(d)).

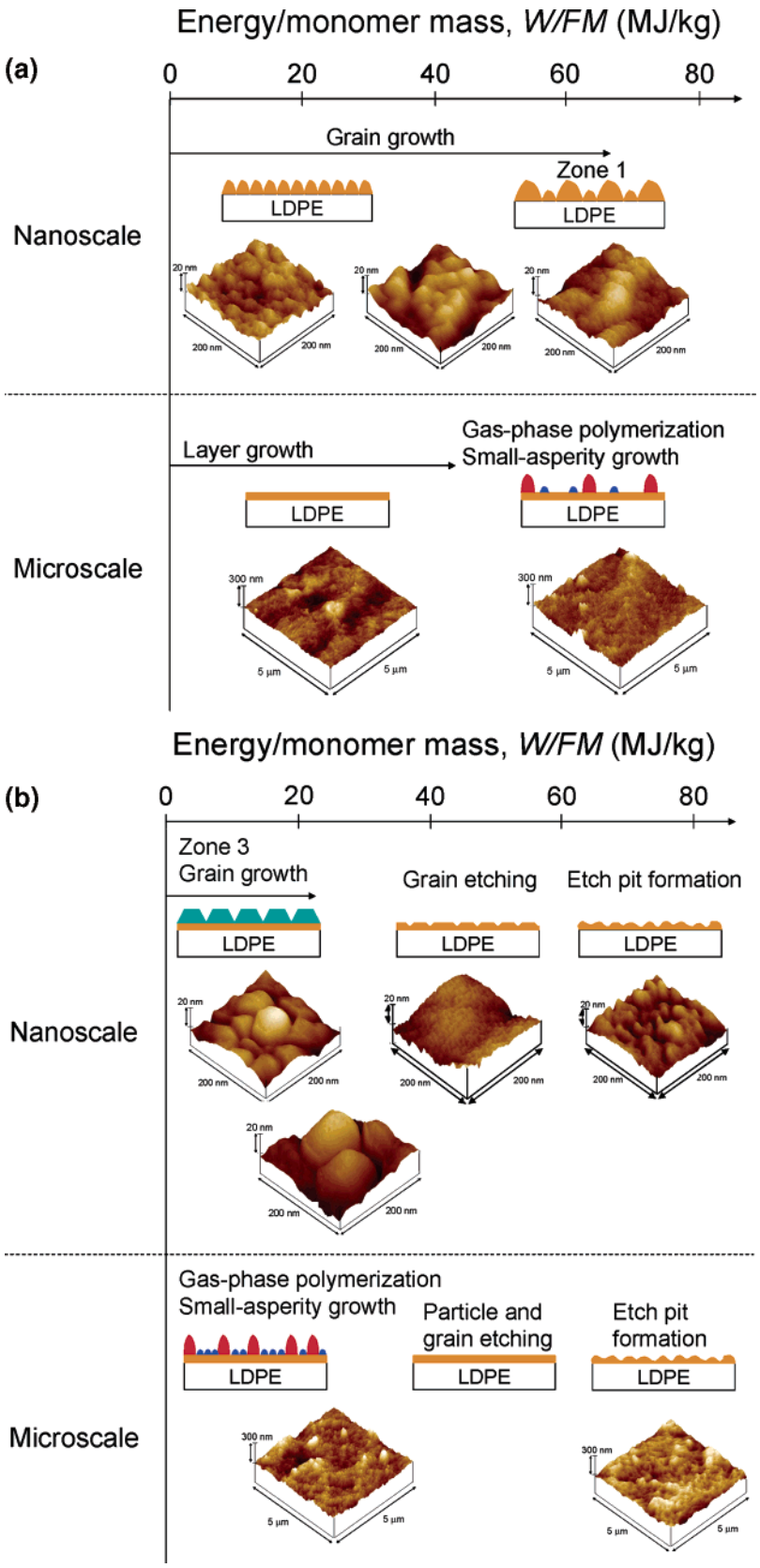

Figure 8. Fluorocarbon film growth mechanisms under (a) shielded and (b) unshielded plasma conditions for different energy/monomer mass. The *x*-coordinate of the upper corner of each AFM image indicates the approximate *W*/*FM* value of the corresponding surface topography.

The grain growth mechanisms under shielded and unshielded plasma conditions observed in Figures 5−7 are presented in the form of nanoscale and microscale growth maps in Figure 8. These maps demonstrate the significance of different plasma species, such as ions, VUV/UV radiation, and uncharged particles on the FC film morphology in terms of energy/monomer mass and feature scale. For shielded plasma conditions, the film growth characteristics are similar to those of the zone 1 growth

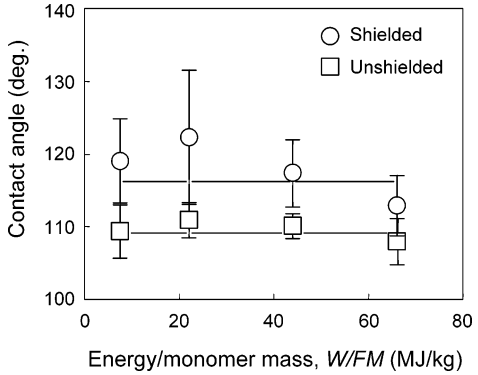

Figure 9. Static contact angle of fluorocarbon films grown under (O) shielded and (□) unshielded plasma conditions versus energy/monomer mass.

model, while for unshielded plasma conditions film growth resembles that of the zone 3 growth model.[33]

Film Hydrophobicity. Figure 9 shows that the static contact angles of the FC films were higher than those of Ar-treated LDPE (33.7 ± 5.9°). The greater scatter in the contact angle data for shielded plasma conditions at relatively low *W/FM* values is attributed to the incomplete surface coverage by the deposited thin films (Table 1). The high contact angles shown in Figure 9 are indicative of the hydrophobicity of the FC films. Shielded plasma conditions produced more hydrophobic film surfaces than unshielded plasma conditions, possibly due to CF_2 enrichment of the films. The low degree of crosslinking in the absence of ion bombardment and VUV/UV radiation effects (shielded plasma conditions) resulted in CF_2-rich films (Figure 1(a)). This postulate is supported by the results of the FC film chemical composition presented in the following section. In view of the statistical error, it may be inferred that the data of Figure 9 reveal a marginal effect of the energy/monomer mass on the hydrophobic behavior of FC films grown under these plasma conditions.

The contact angle measurements could be affected by the surface roughness. Usually, rough surfaces yield higher contact angles than smooth surfaces of the same chemical composition. The surface roughness effect on the contact angle can be interpreted in terms of the roughness factor, defined as the ratio of the true surface area to the apparent area of the imaged surface.[35−38] The very small roughness factors (<1.6) of both microscale and nanoscale topographies indicated that the formation of particles and asperities (Figure 5(c)), etch pits (Figures 5(d) and 7(d)), and grains (Figures 6 and 7) exhibited a secondary effect on the contact angle measurements.

Film Surface Chemistry. Figure 10 shows the effect of energy/monomer mass on the C1s core level XPS spectra of the FC films. The main feature in the spectra for shielded plasma conditions (Figure 10(a)) is the dominance of the $\underline{C}F_2$ peak for $W/FM \geq 22.1$ MJ/kg, suggesting the formation of $\underline{C}F_2$-rich films with structures similar to that shown in Figure 1(a). The high intensity of the $\underline{C}$-C peak for $W/FM = 7.4$ and 22.1 MJ/kg is attributed to the LDPE substrate. This peak was present only in the spectra of the thinner films obtained under shielded plasma conditions (Table 1) in which the XPS sampling depth was greater than the film thickness. For $W/FM \geq 44.1$ MJ/kg, the $\underline{C}$-C peak disappeared from the C1s spectrum, confirming the full coverage of the LDPE surface by the thicker FC films grown under those plasma conditions. The similar intensities of the $\underline{C}F_2$, $\underline{C}F$, and $\underline{C}$-CF_n peaks in the C1s spectra for unshielded plasma conditions (Figure 10(b)) reveal a high number of $\underline{C}F$ and $\underline{C}$-CF_n bonds, implying the development of a crosslinked

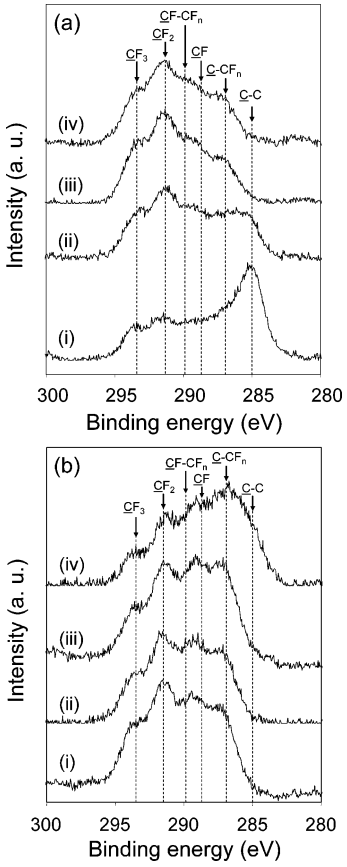

Figure 10. C1s core level XPS spectra of fluorocarbon films grown under (a) shielded and (b) unshielded plasma conditions for (i) $W/FM = 7.4$ MJ/kg, (ii) $W/FM = 22.1$ MJ/kg, (iii) $W/FM = 44.1$ MJ/kg, and (iv) $W/FM = 66.2$ MJ/kg.

film structure similar to that shown in Figure 1(b). In addition, the intensities of the $\underline{C}F$ and $\underline{C}$-CF_n peaks increased with *W/FM* much more than the intensities of the $\underline{C}F_2$ and $\underline{C}F_3$ peaks. This trend illustrates an enhancement of the crosslink density with increasing energy/monomer mass for film deposition under unshielded plasma conditions, consistent with previous results.[22]

Figure 11 shows high-resolution C1s spectra of FC films deposited under shielded and unshielded plasma conditions for $W/FM = 44.1$ MJ/kg. The spectrum shown in Figure 11(a) is similar to that of a FC film grown by the pulsed plasma method.[21] The spectra include GL curve fits at the F-C peak positions given in Table 2. Results for the chemical bonds, F/C ratio, crosslinking percentage, and connectivity number are given in Table 4. The results presented in Figure 11 and Table 4 show that the films deposited under unshielded plasma conditions possessed higher concentrations of $\underline{C}F$ and $\underline{C}$-CF_n bonds, whereas shielded plasma conditions produced films with higher CF_2 and CF_3 contents. In addition, unshielded plasma conditions yielded lower F/C ratio, higher percentage of crosslinking, and higher connectivity number than shielded plasma conditions. These results provide further evidence that unshielded plasma conditions resulted in more crosslinked films (Figure 1(b)), while shielded plasma conditions favored the deposition of CF_2-rich films with less crosslinked structures (Figure 1(a)). Hence, the higher contact angles for shielded plasma conditions (Figure 9) can be attributed to the formation of films with higher CF_2 concentrations. These findings illustrate the important roles of ion bombardment and VUV/UV radiation in FC film crosslinking and are in agreement with the results of a previous study on the effect of plasma species on polymer crosslinking.[19]

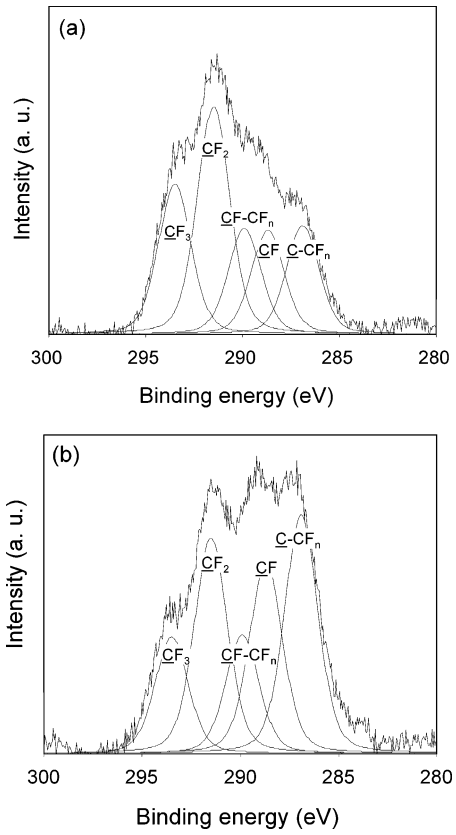

Figure 11. High-resolution C1s core level XPS spectra of fluorocarbon films grown under (a) shielded and (b) unshielded plasma conditions for $W/FM = 44.1$ MJ/kg. (Curve fitting was based on the peak positions given in Table 2.)

TABLE 4: Chemical Bonding, F/C Ratio, Percentage of Crosslinking, and Connectivity Number Obtained from High-Resolution C1s Core Level XPS Spectra of Fluorocarbon Films Grown under Shielded and Unshielded Plasma Conditions[a]

measurement		shielded plasma conditions		unshielded plasma conditions
		2 min	30 min	2 min
chemical bond (%) (Figure 11)	$-\underline{C}F_3$	21.6	22	13.3
	$-\underline{C}F_2-$	32.6	39	24.5
	$-\underline{C}F-CF_n-$	15.2	13.2	13.5
	$-\underline{C}F-$	15.0	14.2	21.7
	$-\underline{C}-CF_n-$	15.5	11.6	27.1
	$-\underline{C}-C-$	0	0	0
F/C ratio (eq 2)		1.60	1.71	1.24
crosslinking X (%) (eq 3)		46	39	62
connectivity m (eq 4)		2.39	2.29	2.76

[a] Energy/monomer mass = 44.1 MJ/kg; deposition time = 2 or 30 min.

Table 4 shows that the film grown in 2 min under shielded plasma conditions exhibited 46% crosslinking, suggesting that the film chemical structure might be a mixture of those shown in Figure 1. However, the data for 30 min deposition time and same plasma conditions indicate that the F/C ratio increased and the crosslink density and connectivity number decreased with the increase of the deposition time. In view of this finding, it may be inferred that the interfacial chemical structure was a mixture of the chemical structures depicted in Figure 1(a) and (b), while the chemical structure of the outer layer of the film resembled that shown in Figure 1(a). The presumed structure

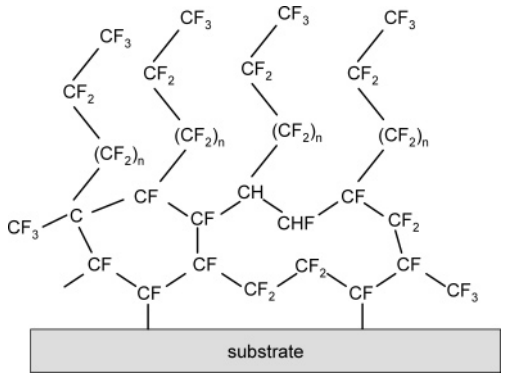

Figure 12. Model of the chemical structure of a hybrid fluorocarbon film grown under shielded plasma conditions.

of this hybrid film is shown in Figure 12. Such a growth model is plausible because in the absence of ion bombardment and VUV/UV radiation the conditions were conducive to the growth of CF_2-rich films, especially for relatively long deposition time. In addition to the higher hydrophobicity of the films grown under shielded plasma conditions, the lower connectivity number might be indicative of the formation of FC chains with increased flexibility. The combination of a crosslinked (strong) interfacial region and a compliant surface layer are beneficial to the bonding strength and surface lubricity of the FC films. These properties are highly desirable for polymer implants and biodevices interacting with soft tissue. Therefore, polymer treatment with uncharged particles alone is especially advantageous for biological applications requiring durable, hydrophobic, and lubricious (low friction) surface coatings.

In this study, FC films with significantly different chemical structures were obtained in the presence of energetic ion bombardment and VUV/UV radiation. The simultaneous effects of these plasma species resulted in the formation of crosslinked FC films, as evidenced by the increase of the $\underline{C}F$ and $\underline{C}$-CF_n peak intensities in the C1s spectrum (Figure 11(b)) and the lower F/C ratio, higher crosslink percentage, and higher connectivity number (Table 4). Ion bombardment and VUV/UV radiation resulted in the abstraction of F from the FC chains, leading to the formation of radicals that reacted with each other to produce three-dimensional crosslink networks in the film structure. Hence, the C-F bonds in the films grown under unshielded plasma conditions produced a structure similar to that shown in Figure 1(b), characterized by greatly reduced chain mobility. As these films are stiffer than those obtained from uncharged particles alone, they are suitable for applications involving high surface shear rates, such as FC films used to lubricate hard disks of magnetic recording drives.

Conclusions

The growth mechanisms of thin FC films synthesized under conditions resulting in surface interaction with uncharged particles only (shielded plasma conditions) or ion bombardment and VUV/UV radiation in conjunction with uncharged particles (unshielded plasma conditions) were analyzed in the context of results for the film thickness, morphology, wettability, and surface chemistry obtained for different values of energy/monomer mass.

The film growth rate exhibited strong dependence on the density and energy of ions as well as the density of uncharged particles generated from the plasma and ion−shield surface collisions. The latter particles contributed significantly to the film growth process under shielded plasma conditions. Different

film growth mechanisms were found under the effect of uncharged particles alone and under the simultaneous effects of ion bombardment, VUV/UV radiation, and uncharged particles from the plasma over a wide range of energy/monomer mass. Microscale film growth comprised the initial deposition of a layer covalently bonded to the polymer substrate, followed by the formation of islands of small asperities and large particles produced from gas-phase polymerization. Nanoscale film growth was characterized by the enlargement of surface grains with the increase of plasma intensity. The FC films deposited under shielded plasma conditions and high energy/monomer mass exhibited zone 1 growth structure, while those deposited under unshielded plasma conditions exhibited either zone 3 growth structure (energy/monomer mass less than a threshold value) or grain removal by plasma etching (energy/monomer mass above a critical value).

Contact angle results demonstrated higher film hydrophobicity for shielded plasma conditions and negligible roughness effect on the contact angle measurements. XPS analysis showed that FC films grown under shielded plasma conditions exhibited less crosslinking and higher CF_2 concentrations than those grown under unshielded plasma conditions. Chemical analysis revealed that thin FC films with hybrid chemical structures consisting of a crosslinked (strong) interfacial layer and a CF_2-rich hydrophobic and compliant surface layer can be grown on polymer surfaces under shielded plasma conditions. The capability to tailor the FC film structure and chemical composition is intriguing and of great importance to biotechnology and various microdevice applications in which control of the surface properties is critical to reliability and performance.

Acknowledgment. This research was funded by the National Science Foundation under Grant No. CMS-0528506.

References and Notes

(1) Stoffels, W. W.; Stoffels, E.; Tachibana, K. *J. Vac. Sci. Technol. A* **1998**, *16*, 87.
(2) Sasaki, K.; Takizawa, K.; Takada, N.; Kadota, K. *Thin Solid Films* **2000**, *374*, 249.
(3) Cunge, G.; Booth, J. P. *J. Appl. Phys.* **1999**, *85*, 3952.
(4) Miyata, K.; Hori, M.; Goto, T. *Jpn. J. Appl. Phys.* **1997**, *36*, 5340.
(5) d'Agostino, R.; Favia, P.; Fracassi, F. *J. Polym. Sci., Part A: Polym. Chem.* **1990**, *28*, 3387.
(6) Li, X.; Hua, X.; Ling, L.; Oehrlein, G. S.; Barela, M.; Anderson, H. M. *J. Vac. Sci. Technol. A* **2002**, *20*, 2052.
(7) Zheng, L.; Ling, L.; Hua, X.; Oehrlein, G. S.; Hudson, E. A. *J. Vac. Sci. Technol. A* **2005**, *23*, 634.
(8) Labelle, C. B.; Opila, R.; Kornblit, A. *J. Vac. Sci. Technol. A* **2005**, *23*, 190.
(9) Favia, P.; Perez-Luna, V. H.; Boland, T.; Castner, D. G.; Ratner, B. D. *Plasmas Polym.* **1996**, *1*, 299.
(10) Kiaei, D.; Hoffman, A. S.; Hanson, S. R. *J. Biomed. Mater. Res.* **1992**, *26*, 357.
(11) Kiaei, D.; Hoffman, A. S.; Horbett, T. A.; Lew, K. R. *J. Biomed. Mater. Res.* **1995**, *29*, 729.
(12) Jaszewski, R. W.; Schift, H.; Schnyder, B.; Schneuwly, A.; Gröning, P. *Appl. Surf. Sci.* **1999**, *143*, 301.
(13) Yasuda, H.; Hirotsu, T. *J. Polym. Sci., Polym. Chem. Ed.* **1978**, *16*, 743.
(14) Yasuda, H.; Wang, C. R. *J. Polym. Sci., Polym. Chem. Ed.* **1985**, *23*, 87.
(15) Sandrin, L.; Silverstein, M. S.; Sacher, E. *Polymer* **2001**, *42*, 3761.
(16) Chen, R.; Gorelik, V.; Silverstein, M. S. *J. Appl. Polym. Sci.* **1995**, *56*, 615.
(17) Tajima, S.; Komvopoulos, K. *J. Phys. Chem. B* **2005**, *109*, 17623.
(18) Tajima, S.; Komvopoulos, K. *J. Phys. D: Appl. Phys.* **2006**, *39*, 1084.
(19) Tajima, S.; Komvopoulos, K. *Appl. Phys. Lett.* **2006**, *89*, 124102.
(20) Martin, I. T.; Fisher, E. R. *J. Vac. Sci. Technol. A* **2004**, *22*, 2168.
(21) Martin, I. T.; Malkov, G. S.; Butoi, C. I.; Fisher, E. R. *J. Vac. Sci. Technol. A* **2004**, *22*, 227.
(22) Labelle, C. B.; Donnelly, V. M.; Bogart, G. R.; Opila, R. L.; Kornblit, A. *J. Vac. Sci. Technol. A* **2004**, *22*, 2500.
(23) Clark, D. T. In *Photon, Electron and Ion Probes of Polymer Structure and Properties*; Dwight, D. W., Fabish, T. J., Thomas, H. R., Eds.; American Chemical Society: Washington, D.C., 1981; pp. 247−291.
(24) Horie, M. *J. Vac. Sci. Technol. A* **1995**, *13*, 2490.
(25) Fuoco, E. R.; Hanley, L. *J. Appl. Phys.* **2002**, *92*, 37.
(26) Winder, E. J.; Gleason, K. K. *J. Appl. Polym. Sci.* **2000**, *78*, 842.
(27) Garrison, M. D.; Luginbühl, R.; Overney, R. M.; Ratner, B. D. *Thin Solid Films* **1999**, *352*, 13.
(28) He, H.; Thorpe, M. F. *Phys. Rev. Lett.* **1985**, *54*, 2107.
(29) Döhler, G. H.; Dandoloff, R.; Bilz, H. *J. Non-Cryst. Solids* **1980**, *42*, 87.
(30) Silverstein, M. S.; Chen, R.; Kesler, O. *Polym. Eng. Sci.* **1996**, *36*, 2542.
(31) Coburn, J. W.; Winters, H. F. *J. Vac. Sci. Technol.* **1979**, *16*, 391.
(32) Ohring, M. *Materials Science of Thin Films, Deposition and Structure*, 2nd ed.; Academic Press: San Diego, CA, 2002.
(33) Thornton, J. A. *Annu. Rev. Mater. Sci.* **1977**, *7*, 239.
(34) Labelle, C. B.; Gleason, K. K. *J. Appl. Polym. Sci.* **1999**, *74*, 2439.
(35) Wenzel, R. N. *Ind. Eng. Chem.* **1936**, *28*, 988.
(36) Wenzel, R. N. *J. Phys. Colloid. Chem.* **1949**, *53*, 1466.
(37) Johnson, R. E., Jr.; Dettre, R. H. *Adv. Chem. Ser.* **1964**, *43*, 112.
(38) Cassie, B. D.; Baxter, S. *Trans. Faraday Soc.* **1944**, *40*, 546.